Interplay of Wetting and Elasticity in the Nucleation of Carbon Nanotubes

Dmitri Schebarchov,[1] Shaun C. Hendy,[1,2] Elif Ertekin,[3] and Jeffrey C. Grossman[3]

[1]*MacDiarmid Institute for Advanced Materials and Nanotechnology, Industrial Research Ltd, Lower Hutt 5040, New Zealand*
[2]*School of Chemical and Physical Sciences, Victoria University of Wellington, Wellington 6140, New Zealand*
[3]*Department of Materials Science and Engineering, Massachusetts Institute of Technology, Cambridge, Massachusetts 02139, USA*

(Received 1 May 2011; published 27 October 2011)

We use molecular dynamics and simple thermodynamic arguments to model the interaction between catalyst nanoparticles and carbon nanotube caps, and we illustrate how the competition between cap strain energy and adhesion plays a role in the lifting of these caps from the catalyst surface prior to tube elongation. Given a particular cap structure, we show that there is a lower bound on the catalyst size from which the cap can lift. This lower bound depends on the cap's spontaneous curvature and bending rigidity, as well as the catalyst binding strength, and it explains the mismatch between single-walled carbon nanotube and catalyst diameters observed in prior experiments. These findings offer new insight into the nucleation of carbon nanotubes, and they may lead to the design of catalysts that can better control nanotube structure.

DOI: 10.1103/PhysRevLett.107.185503 PACS numbers: 61.48.De, 68.35.Np

Controlling the structure of single-walled carbon nanotubes (SWCNTs) [1] during synthesis is one of the outstanding challenges of nanoscale science [2,3]. Using catalytic synthesis, one of the most promising routes to controlled growth of carbon nanotubes, it is possible to bias the diameter [4–8] and chirality [9,10] distributions of as-grown SWCNTs by altering the structure and composition of the catalyst, but whether this approach can be fine-tuned to attain the desired level of selectivity remains unclear [3]. After two decades of investigation, it seems likely that this uncertainty will only be resolved through a deeper understanding of the catalyst-nanotube interactions, particularly during the nucleation stage.

One prominent school of thought holds that the final structure of a catalytically grown SWCNT is to a large degree determined by the initial graphitic cap [10,11], or *yarmulke*, which must first nucleate on the catalyst surface and then lift-off to allow the tube to elongate. Though the process of cap nucleation and lift-off has been observed *in situ* [12] and simulated using a number of theoretical methods [13], a clear link between the structure of a nucleating SWCNT and that of the parent catalyst is yet to emerge. In search of that link, here we model the interaction between particular caps and a range of catalyst particles using classical molecular dynamics and continuum arguments. Note that our intention is not to accurately simulate nanotube nucleation, but rather to contrive a simple framework that will elucidate the key physical parameters that dictate cap lift-off. Identifying these parameters is an important step towards selective nanotube growth, as it could help with the design of catalysts that favor lift-off only of caps that lead to tubes of specific chirality or radius.

We begin by considering a prototypical tube nucleus, C30 (half of a C60 fullerene), on the surface of a spherical catalyst (see Fig. 1). Carbon-carbon interactions are modeled with the Tersoff potential [14], and the binding of carbon atoms to the catalyst surface is modeled using a shifted Lennard-Jones field:

$$U_{\mathrm{LJ}}(\tilde{r}) = U(\tilde{r}) - U(r_c) + (\tilde{r}/r_c - 1)(dU/d\tilde{r})|_{\tilde{r}=r_c},$$

where $U(\tilde{r}) = 4\varepsilon_s\varepsilon_i[(\sigma/\tilde{r})^{12} - (\sigma/\tilde{r})^6]$, $\tilde{r} \equiv r - R + 2^{1/6}\sigma$, $r_c = 3.2\sigma$, $\sigma = 1$ Å, ε_s is a dimensionless prefactor, and R is the adjustable catalyst radius. The values of ε_i, with i denoting the carbon atom coordination, were matched to *ab initio* calculations of graphene flakes on the fcc Fe(100) surface: $\varepsilon_2 = 0.78$ eV and $\varepsilon_3 = 0.13$ eV. These values were uniformly scaled by ε_s to adjust the net binding strength (with $\varepsilon_s = 1$ restoring the *ab initio* matched values). This model is not intended to provide a quantitatively accurate representation of the actual system, rather it allows us to easily adjust catalyst characteristics such as R and ε_s and observe their effect on the equilibrium state of a particular cap. More specifically, we can use the model to artificially induce lift-off of the catalyst-supported C30 by gradually increasing R. Lift-off can then be characterized through the variation in equilibrium Tersoff (E_T) and Lennard-Jones (E_{LJ}) energies of the cap while R increases, as shown in Fig. 2.

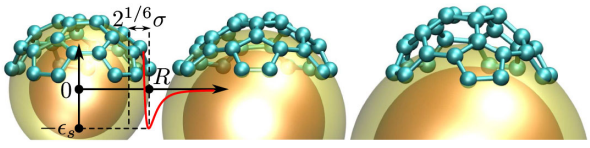

FIG. 1 (color online). Ball-and-stick representation of C30 on spherical (Lennard-Jones) catalysts. Yellow outer spheres represent the catalyst radius R, and orange inner spheres correspond to $R - 2^{1/6}\sigma$ where there is infinite repulsion.

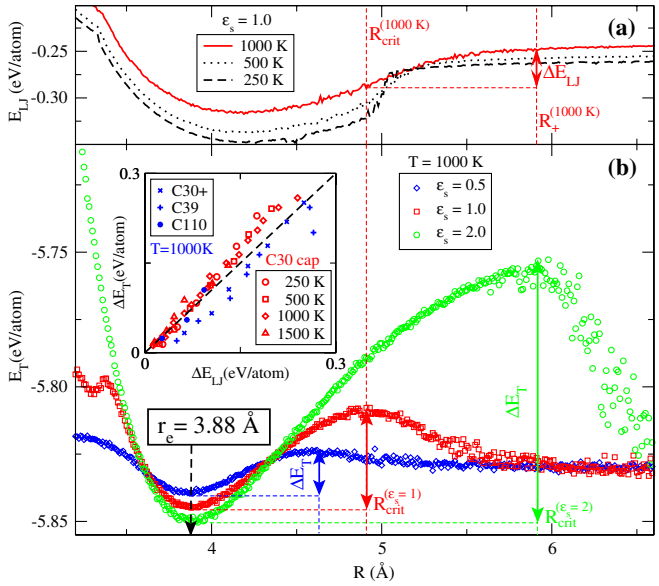

FIG. 2 (color online). Variation in cohesive (E_T) and adhesive (E_{LJ}) energies of C30 as R increases from 3.2 Å to 7.2 Å in increments of 0.01 Å. Note that in (a) E_{LJ} is plotted versus R for $\varepsilon_s = 1$ at three different temperatures; and in (b) E_T is plotted versus R at 1000 K for three different values of ε_s. All the $E_T(R)$ and $E_{LJ}(R)$ values were equilibrated and averaged over 10^5 time steps (0.5 fs each). We find the trends to be reversible—subsequent gradual shrinking of R yields the same behavior. Adjusting the temperature has some effect on the general shape of the trends, with the lift-off transition being sharper at lower temperatures, but the location of r_e and R_{crit} remains largely unchanged. $E_T(R)$ and $E_{LJ}(R)$ remain roughly constant for $R > R_+$, where R_+ is typically between R_{crit} and $R_{crit} + 1$ Å. In the inset we plot the maximal strain energy, i.e. $\Delta E_T = E_T(R_{crit}) - E_T(r_e)$, versus the work of adhesion that is overcome during lift-off, i.e., $\Delta E_{LJ} = E_{LJ}(R_+) - E_{LJ}(R_{crit})$. We find $\Delta E_{LJ} \approx \Delta E_T$ for a wide range of temperatures, catalyst binding strengths, and different cap structures (i.e., C30 + , C39 and C110) defined later in the text.

The most distinct features in Fig. 2 are the minima in E_T at $R = r_e$, corresponding to the natural curvature of our prototype cap, and the maxima at $R = R_{crit}(\varepsilon_s) > r_e$ that shift with ε_s. From visual inspection it becomes apparent that the drop in E_T for $R > R_{crit}$ is due to cap lift-off, and it is accompanied by an increase in E_{LJ} of similar magnitude. For $r_e < R < R_{crit}$ the cap (on average) adheres to the catalyst surface and undergoes increasing bending strain and in-plane deformation as its radius of curvature deviates further from r_e. At $R \sim R_+ \gtrsim R_{crit}$ the cap's interior lifts and most of the strain gets released. From now on we shall refer to the range $R > R_{crit}$ as the *lifted* state and $R < R_{crit}$ as the *collapsed* state. Note that $\Delta E_T \sim \Delta E_{LJ} \sim 70$ meV/atom for $\varepsilon_s = 1$ is comparable to $k_B T \sim 90$ meV at 1000 K, so it is necessary to consider time-averaged energies to attain the characteristic trends in Fig. 2.

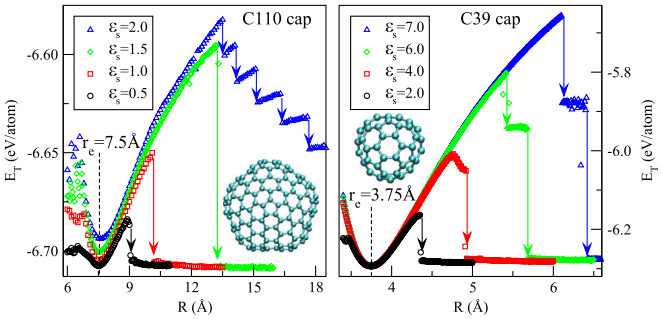

FIG. 3 (color online). E_T versus R for C110 and C39 at 1000 K. Arrows indicate transitions to complete or partial lift-off.

Our simulation scheme can be used to artificially induce lift-off and explore the equilibrium states in any given cap structure. For instance, Fig. 3 shows two different caps, C110 and C39, responding to changes in R and ε_s similarly to C30. Interestingly, in both cases we find that high ε_s leads to multistep lift-off, illustrating how in the strong adhesion limit the transition can be a cascade of partial lift-off events in various sections of the cap. However, setting $\varepsilon_s = 1$ yields single-step lift-off in all three caps, with the ratio R_{crit}/r_e being ~1.3 for C110 and C30 and ~1.1 for C39. These values are comparable to the catalyst-to-nanotube diameter ratios inferred from experiments [4,5], whereas the apparent difference in R_{crit}/r_e between the armchair (i.e., C30 and C110) and the zigzag (i.e., C39) caps suggests that this ratio may be sensitive to the edge structure and, hence, the chiral angle.

So far we have only considered ideal caps, consisting entirely of hexagonal and pentagonal rings and obeying the isolated pentagon rule, but it is also interesting to consider how nonideal caps with localized strain energy might lift-off. Figure 4 illustrates how a single Stone-Wales-type

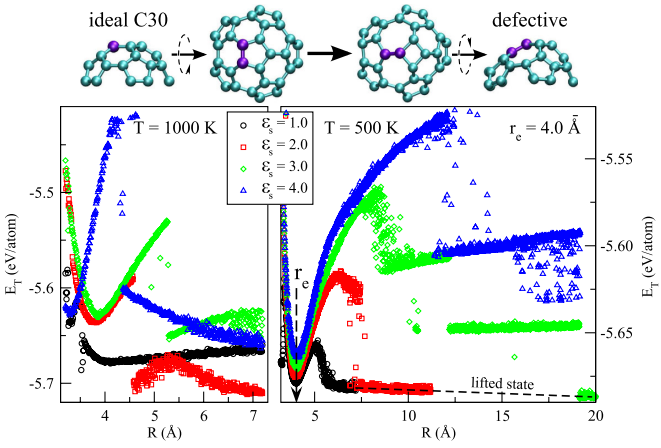

FIG. 4 (color online). E_T versus R for a defective C30 cap. Simulations at 1000 K do not exhibit a consistent trend, whereas those at 500 K do and it is possible to identify the lift-off transition.

rotation alters the topology of C30 and its response to changes in R and ε_s. The dependence of E_T on R is not as clear-cut as it was in Fig. 2, and it is difficult to identify r_e and R_{crit}. The lack of a consistent trend at 1000 K is evidently due to thermally induced distortions around the defect. Running the same simulations at 500 K suppresses these fluctuations, yielding trends that are closer to those of an ideal C30 cap with a characteristic r_e and identifiable lifted state. Simulations with $\varepsilon_s > 2$ exhibit multistep lift-off, something not seen in an ideal C30 cap, but setting $\varepsilon_s = 1$ leads to single-step lift-off with a value of R_{crit}/r_e similar to that of the ideal cap.

To gain further insight into our single-step lift-off simulations, we offer a simple model based on the schematic in Fig. 5. A spherical membrane of (fixed) area A and adjustable radius r represents a graphitic cap with its free edge constrained to the catalyst surface, modeled as a rigid sphere of radius R. Consider how the energy of this system might vary with r in the range $\sqrt{A/(4\pi)} < r \leq R$. First, peeling the cap interior off the catalyst surface (i.e., transition from $r = R$ to $r < R$) increases the total surface energy by $Aw > 0$, where w is the work of adhesion per unit area. Second, in our simulations it was apparent that a given cap structure has some preferred radius of curvature r_e, and adhesion to a spherical catalyst of radius $R > r_e$ resulted in an energy penalty (due to bending) that *favored* lift-off. This competition between adhesion and curvature essentially determines the relative stability of the lifted and collapsed states.

Expanding the curvature energy about the equilibrium (i.e., $r^{-1} = r_e^{-1}$) yields a special case of the Helfrich Hamiltonian [15,16]:

$$E_C(r) = A\kappa(r^{-1} - r_e^{-1})^2, \tag{1}$$

where κ represents bending rigidity. The requirement for lift-off is simply $Aw < E_C(R)$; i.e., the curvature energy penalty associated with the collapsed state ($r = R$) must exceed the work of adhesion. Assuming $r_e \leq R$, this condition leads to a lower bound on the catalyst radius: $R > r_e(1 - r_e/L_C)^{-1}$ where $L_C = \sqrt{\kappa/w}$ is a characteristic length. We can define the critical catalyst radius for a particular r_e:

$$R_{\text{crit}} = r_e(1 - r_e/L_C)^{-1}, \tag{2}$$

such that the lifted state is energetically favored over the collapsed state when $R > R_{\text{crit}}$. Note that Eq. (2) does not yield a physically plausible R_{crit} when $r_e \geq L_C$, in which case the lifted state cannot be thermodynamically stable for *any* $R > 0$. Furthermore, if $r_e < L_C$ then $R_{\text{crit}} \geq r_e$ and the equality only holds in the limit $r_e/L_C \to 0$. The message is more transparent when the lift-off condition is written as $r_e < R(1 + R/L_C)^{-1}$ and, if we take r_e of a lifted cap as the radius of the subsequent SWCNT, it imposes the requirement that the diameter of SWCNTs be smaller than that of the catalyst particles—consistent with the available empirical data. [4–8] The model also implies that nanotubes can grow on *any* catalyst particle above the critical size, which agrees with prior reports of nanotube formation on planar surfaces (i.e., $R \to \infty$). [17]

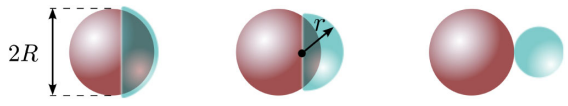

FIG. 5 (color online). Schematic of our continuum model for cap lift-off. The catalyst is a rigid sphere of radius R, and the cap is a thin, spherical membrane of area A and adjustable radius r.

Having obtained an expression for R_{crit}, we can check how well it fits our molecular dynamics simulations. Taking the values of R_{crit} from Fig. 2 and plotting them versus the corresponding work of adhesion ($w \propto \Delta E_{\text{LJ}}$) yields a trend that is well reproduced by Eq. (2), as shown in Fig. 6, with κ being the only free parameter since r_e can be inferred directly from Fig. 2. We find that the fitted value of κ changes with cap structure: for C30 it is similar to the bending rigidity of graphene ($\kappa \sim 1$–2 eV [16,18]); while for C30 + , which has ten more carbon atoms attached so as to preserve the armchair edge structure, κ is almost an order of magnitude larger. This increase in κ means that, as one would expect, the susceptibility to collapse will diminish as a lifted cap elongates into a tube. Note that κ is even greater for C39, which has a zigzag edge, indicating that the bending rigidity is sensitive to edge effects.

An important quantity that emerged from our model is the characteristic length L_C, which essentially determines whether a cap of particular r_e is at all capable of lifting, and if so, then L_C imposes a minimum diameter mismatch between a lifted cap and the catalyst. In our simulations

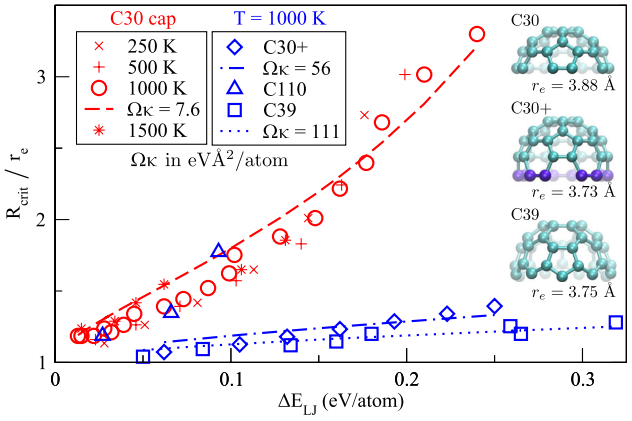

FIG. 6 (color online). The ratio R_{crit}/r_e is shown to increase with the specified work of adhesion (ΔE_{LJ}), and the trends are fitted with Eq. (2). From our simulations of a complete C60 fullerene at 1000 K, we estimate the occupied area per atom $\Omega \sim 3$ Å^2/atom, which yields $\kappa \sim 2.5$ eV for C30. Adding an extra ring of 10 carbon atoms (see C30 +) shifts the trend and raises the rigidity to $\kappa \sim 19$ eV. C39, which has a zigzag edge, is even more rigid with $\kappa \sim 37$ eV.

TABLE I. Estimates of L_C for graphene with $\kappa = 1$ eV and liquid metals with surface tension γ and contact angle θ_c on graphite. We first use Young's relation $w = \gamma(1 + \cos\theta_c)$ and then compute $L_C = \sqrt{\kappa/w}$. Note that carbon contents in $Fe_{79}C_{21}$ and $Ni_{88}C_{12}$ correspond to the saturation limits.

Metal	γ (eV/nm^2)	θ_c	w (eV/nm^2)	L_C (nm)
Fe	11.5 [19]	42° [19]	20	0.2
$Fe_{79}C_{21}$	9.2 [19]	142° [19]	2.0	0.7
Ni	11.4 [21]	50° [20]	19	0.2
$Ni_{88}C_{12}$	8.1 [22]	115° [20]	4.7	0.5
Au	7.1 [23]	129° [23]	2.6	0.6

L_C is cap-dependent and, for $\varepsilon_s = 1$, it ranges from 1.4 nm (for C30) to 3.6 nm (for C39)—comparable to the typical SWCNT diameters. Since these values are subject to change with the accuracy of the model, we also estimate L_C from the measured bending rigidity of graphene ($\kappa \sim$ 1–2 eV [16,18]) and the work of adhesion w inferred from experimental studies of wetting of graphite by various metals [19–22]. These estimates (see Table I) are also comparable to the typical SWCNT diameters, providing more compelling evidence that the competition between (spontaneous) curvature and adhesion must indeed be an important factor in the nucleation of SWCNTs. Note that L_C for $Ni_{88}C_{12}$ is smaller than for $Fe_{79}C_{21}$ (for any κ); hence, using a carbon-saturated Ni catalyst will require a larger particle size than carbon-saturated Fe to ensure caps of particular r_e lift-off. This deduction is consistent with the available experimental data: the catalyst-to-nanotube diameter ratios for as-grown SWCNTs of 1–2 nm diameter have been estimated to be ~2–3 in Ni-catalyzed growth [6,7] and ~1–2 in Fe-catalyzed growth [4,5].

We stress that the key ansatz of our continuum model is the introduction of spontaneous curvature r_e^{-1}, which was simply inferred from molecular dynamics simulations to inform (1). We interpret r_e as an effective parameter that also includes edge effects: It represents the mean (positive) curvature due to pentagonal rings, which can reduce the number of (catalyst-stabilized) dangling bonds in a graphene flake [24,25], and it can also arise due to a particular angular preference in the overlap of the unsaturated sp^2 carbon and the catalyst orbitals [25,26]. Ideally, we want to move to a model where the cap details are not subsumed into an effective r_e. A more explicit treatment of edge effects is particularly desirable, as it may allow one to model nanotube chirality during lift-off [27].

Finally, it is worth reiterating that here we had assumed a rigid catalyst and a flexible cap. Our prior model [28] for capillary uptake of droplets by nanotubes considers the opposite limit of "relative rigidity"—there the SWCNT is rigid and the catalyst is fluid—and that analysis also leads to a critical catalyst radius $R^\dagger$. A catalyst of radius $R < R^\dagger$ will fill the void and wet the interior of a rigid tube nucleus via capillary forces. This refilling will occur spontaneously for contact angles $\theta_c < 90°$, regardless of catalyst size, unless the nanotube growth kinetics is significantly faster than catalyst reshaping. Hence, a necessary condition for cap lift-off is not only $R > R_{\text{crit}}$, but also $\theta_c > 90°$ and $R > R^\dagger$. Interestingly, *pure* Fe, Ni and Co (not shown in Table I) have a relatively strong affinity for graphite ($\theta_c < 60°$) that diminishes with carbon dissolution, which suggests that it may be necessary for these metals to absorb carbon feedstock in order to reduce adhesion between the cap and the catalyst.

To summarize, we used relatively simple models to explain what drives the lifting of catalyst-supported carbon nanotube caps prior to tube elongation. By interpreting cap lift-off as arising from the competition between cap strain energy and cap-catalyst adhesion, we identified two key parameters: The effective cap curvature r_e^{-1}, which is a feature of the particular cap structure, and the characteristic length L_C, which depends on the catalyst binding strength and the bending rigidity of the cap. We showed that L_C imposes the requirement that the radius of lifted caps be smaller than that of the catalyst, which explains the observed diameter mismatch between SWCNTs and the catalyst particles. These findings serve as a first step towards a more predictive model for carbon nanotube growth. They also show that cap lift-off is sensitive to cap structure and, hence, suggest that a chirality-selective growth process could yet be designed.

This work was supported by the Royal Society of New Zealand Marsden Fund Contract No. IRL0602, the MacDiarmid Institute for Advanced Materials and Nanotechnology, the Ministry of Research Science and Technology, and Fulbright NZ. DFT calculations were performed at TeraGrid supercomputing facilities.

[1] S. Iijima and T. Ichihashi, Nature (London) **363**, 603 (1993); D. S. Bethune *et al.*, *ibid.* **363**, 605 (1993).
[2] R. Baughman, A. Zakhidov, and W. De Heer, Science **297**, 787 (2002).
[3] M. Hersam, Nature Nanotech. **3**, 387 (2008).
[4] A. G. Nasibulin, P. V. Pikhitsa, H. Jiang, and E. I. Kauppinen, Carbon **43**, 2251 (2005).
[5] D. Kondo, S. Sato, and Y. Awano, Chem. Phys. Lett. **422**, 481 (2006).
[6] M. Paillet *et al.*, J. Phys. Chem. B **108**, 17112 (2004).
[7] K. Kakehi, S. Noda, S. Chiashi, and S. Maruyama, Chem. Phys. Lett. **428**, 381 (2006).
[8] G.-H. Jeong *et al.*, Appl. Phys. Lett. **90**, 043108 (2007).
[9] S. Bachilo *et al.*, J. Am. Chem. Soc. **125**, 11 186 (2003).
[10] W. Chiang and R. Sankaran, Nature Mater. **8**, 882 (2009).
[11] H. Dai *et al.*, Chem. Phys. Lett. **260**, 471 (1996); Y. Miyauchi, S. Chiashi, Y. Murakami, Y. Hayashida, and S. Maruyama, *ibid.* **387**, 198 (2004); S. Reich, L. Li, and J. Robertson, *ibid.* **421**, 469 (2006); H. Kanzow, C. Lenski, and A. Ding, Phys. Rev. B **63**, 125402 (2001).
[12] J. Rodríguez-Manzo *et al.*, Nature Nanotech. **2**, 307 (2007); S. Hofmann *et al.*, Nano Lett. **7**, 602 (2007); H.

Yoshida, S. Takeda, T. Uchiyama, H. Kohno, and Y. Homma, *ibid.* **8**, 2082 (2008).
[13] Y. Shibuta and S. Maruyama, Chem. Phys. Lett. **382**, 381 (2003); F. Ding, K. Bolton, and A. Rosen, J. Phys. Chem. B **108**, 17 369 (2004); J.-Y. Raty, F. Gygi, and G. Galli, Phys. Rev. Lett. **95**, 096103 (2005); H. Amara, C. Bichara, and F. Ducastelle, *ibid.* **100**, 056105 (2008).
[14] J. Tersoff, Phys. Rev. B **39**, 5566 (1989).
[15] W. Helfrich, Z. Naturforsch. B **28**, 693 (1973).
[16] Z. Tu and Z. Ou-Yang, J. Comput. Theor. Nanosci. **5**, 1192 (2008).
[17] S. Irle, Z. Wang, G. Zheng, K. Morokuma, and M. Kusunoki, J. Chem. Phys. **125**, 044702 (2006).
[18] A. Fasolino, J. Los, and M. Katsnelson, Nature Mater. **6**, 858 (2007).
[19] V. Nizhenko and L. Floka, Powder Metallurgy and Metal Ceramics **13**, 487 (1974).
[20] Y. V. Naidich, V. M. Perevertailo, and G. M. Nevodnik, Powder Metallurgy and Metal Ceramics **10**, 45 (1971).
[21] F. Xiao, L. Fang , and K. Nogi, J. Mater. Sci. Technol. **21**, 201 (2005).
[22] V. I. Nizhenko and L. I. Floka, Powder Metallurgy and Metal Ceramics **39**, 462 (2000).
[23] J. Lee *et al.*, Rare Metals **25**, 469 (2006).
[24] A. Chuvilin, U. Kaiser, E. Bichoutskaia, N. Besley, and A. Khlobystov, Nature Chem. **2**, 450 (2010).
[25] X. Fan *et al.*, Phys. Rev. Lett. **90**, 145501 (2003).
[26] B. Wang, X. Ma, M. Caffio, R. Schaub, and W.-X. Li, Nano Lett. **11**, 424 (2011).
[27] Y. Liu, A. Dobrinsky, and B. I. Yakobson, Phys. Rev. Lett. **105**, 235502 (2010).
[28] D. Schebarchov and S. C. Hendy, Nano Lett. **8**, 2253 (2008); **9**, 3668 (2009); Nanoscale **3**, 134 (2011).